DOI: 10.1021/cg9005778

CRYSTAL GROWTH & DESIGN Article

2009, Vol. 9
4567–4573

Novel Method to Estimate the Linear Growth Rate of Submicrometric Calcite Produced in a Triphasic Gas−Liquid−Solid System

G. Montes-Hernandez,*[,†,⊥] A. Fernández-Martínez,[†,‡] and F. Renard[§,⊥]

[†]*Université J. Fourier - Grenoble I/CNRS/LGIT, BP 53, 38041 Grenoble, France,* [‡]*Institut Laue-Langevin, B.P. 156, 38042 Grenoble Cedex 9, France,* [§]*Physics of Geological Processes, University of Oslo, Norway, and* [⊥]*Université J. Fourier - Grenoble I/CNRS/LGCA, BP 53, 38041 Grenoble, France*

Received May 28, 2009; Revised Manuscript Received August 13, 2009

ABSTRACT: The linear growth rate is an essential parameter to describe and simulate the crystal growth processes of solid materials. Concerning the calcite mineral, indirect methods (by depletion of calcium concentration) and direct methods (ex. using microscopic measurements) have been reported in the literature. Here, homogeneous (solution−solution) or heterogeneous (solution−solid) systems are systematically considered. Conversely, the estimation of linear growth rate of calcite for the triphasic gas−liquid−solid systems under high gas pressure and temperature has not been reported in the literature to the best of our knowledge. In the present study, we propose a new method to estimate the linear growth initial rate of submicrometric calcite produced in a triphasic gas−liquid−solid system under high gas pressure (55 and 90 bar) and moderated to high temperature (30 and 90 °C) by using Rietveld refinements of X-ray diffraction (XRD) patterns. These Rietveld refinements allowed the estimation on the variation of the coherent domain average size r (nm) with reaction time t (s). Then, a kinetic pseudo-second-order model was satisfactory used to fit the experimental−calculated data and determine the linear growth initial rate of submicrometric calcite. The results showed that the values of linear growth rate of calcite were equivalents for both systems, i.e., 0.14 nm/s at 30 °C and 55 bar and 0.12 nm/s at 90 °C and 90 bar. However, the average size of calcite crystals, here expressed as a maximum of coherent domain average size, was clearly higher at 90 °C and 90 bar (174 nm) than at 30 °C and 55 bar (63 nm). The main advantage for this method is the possibility to estimate the linear growth rate of crystalline fine particles (> 40 nm) growing in triphasic gas−liquid−solid systems. Here, it is considered that depressurization of cell reaction has insignificant physicochemical effect on the solid precipitates; obviously, this is not the case for the interacting solutions.

1. Introduction

The natural weathering processes of calcium or magnesium silicates, frequent in the Earth's crust produce solid particles and ions that are transported via the rivers to the lakes and oceans. For example, the global hydrolysis reaction of a calcium pyroxene can be expressed as

$$CaSiO_3(s)+H_2O(l)+2CO_2(aq) \rightarrow SiO_2(aq\ or\ s)+Ca^{2+}+2HCO_3^- \quad (1)$$

In the lakes or oceans, the HCO_3^- ions can precipitate as carbonates via chemical or biogenic routes

$$Ca^{2+}+2HCO_3^- \leftrightarrow CaCO_3(s)+H_2O(l)+CO_2(aq\ or\ g) \quad (2)$$

The natural weathering of alkaline silicates followed by carbonates formation consumes carbon dioxide and represents therefore a clear example of natural mineralization of CO_2

$$CaSiO_3(s)+CO_2(aq) \rightarrow SiO_2(aq\ or\ s)+CaCO_3(s) \quad (3)$$

This fundamental concept supports the possibility to storage permanently anthropogenic CO_2 into geological formations (in situ mineral sequestration of CO_2) in order to reduce the carbon dioxide emissions into the atmosphere, which are directly associated with global warming.[1,2] In the last decades, the ex situ mineral sequestration of CO_2 (controlled industrial reactors) has been also proposed to contribute on the reduction of CO_2 emissions into atmosphere. For this case the natural alkaline minerals or alkaline solid−liquid waste (municipal-waste combustion fly ash, bottom ash, brine alkaline solutions, waste concrete and cements, steel slag, coal combustion fly ash, alkaline paper mill waste, asbestos, etc.) can be used to mineralize the CO_2.[3−7] Obviously, the capacity to sequester CO_2 using alkaline residues depends directly on the proportion and chemical-availability of binary oxides (CaO and MgO) and/or hydroxides ($Ca(OH)_2$ and $Mg(OH)_2$) contained in the waste matrix. Conversely, when the natural alkaline minerals are used as reactants, the mineralization of CO_2 is mainly controlled by the dissolution process of these reactants. Obviously, the in situ or ex-situ sequestration of CO_2 involve generally the triphasic gas−liquid−solid systems under hydrothermal or solvothermal conditions. For example, the reaction mechanism of calcite precipitation via aqueous carbonation of $Ca(OH)_2$ in a triphasic gas−liquid−solid system is described by the global exothermic reaction[8]

$$Ca(OH)_2(s)+CO_2(aq) \rightarrow CaCO_3(s)+H_2O(l) \quad (4)$$

that concerns the spontaneous chemical dissolution of $Ca(OH)_2$

$$Ca(OH)_2(s) \xrightarrow{water} Ca^{2+}+2OH^- \quad (5)$$

and a complete dissociation of dissolved CO_2 due to alkaline conditions in interacting solution. Note that the

*Corresponding author. E-mail: german.montes-hernandez@obs.ujf-grenoble.fr; german_montes@hotmail.com.

Published on Web 09/01/2009

alkaline conditions are in situ produced by the dissolution of calcium hydroxide (pH > 10.2),

$$CO_2(aq)+H_2O_{(l)} \rightarrow {CO_3}^{2-}+2H^+ \quad (6)$$

these processes producing a fast supersaturation of solution with respect to calcite and then a spontaneous nucleation of calcite (formation of nuclei or critical cluster)

$$Ca^{2+}+{CO_3}^{2-} \rightarrow CaCO_3(\text{s nuclei}) \quad (7)$$

Finally, crystal growth occurs spontaneously until a thermodynamic equilibrium between calcite and the solution is reached in this closed system

$$CaCO_3(\text{s nuclei}) \rightarrow CaCO_3(\text{s calcite}) \quad (8)$$

As a consequence, the aqueous formation of carbonates in natural or artificial systems depends mainly on the physicochemical parameters such as supersaturation degree, pH, P_{CO2}, temperature, ionic force, fluid composition, pressure, and presence of impurities. It also depends on the hydrodynamics (discontinuous or continuous reactors and static or stirred conditions) and nature (homogeneous or heterogeneous reaction and biotic or abiotic formation) of the system. This experimental information has been widely discussed and frequently supported by macroscopic or atomistic models in the literature (see for example refs 9−23). For example, in closed systems involving heterogeneous reactions (solution−solid interfaces), the crystal growth rate is classically determined using the mass growth rate per unit surface area of crystal expressed as follows[24]

$$\frac{1}{A}\frac{dm}{dt} = \frac{\rho_s}{A}\frac{dV_s}{dt} = \frac{3\rho_s f_v}{f_s}\frac{dL}{dt} \quad (9)$$

where A, V_s, and ρ_s are the surface area, volume, and density of seed crystals, respectively. Here, the linear growth rate is related to the mass growth rate by the following equation

$$G = \frac{dL}{dt} = \frac{f_s}{3f_v\rho_s A}\frac{dm}{dt} \quad (10)$$

where mass growth rate, dm/dt, can be estimated from depletion of calcium ion into the interacting solution.

$$\frac{dm}{dt} = MV\left(-\frac{d[Ca^{2+}]}{dt}\right) \quad (11)$$

where M is the molecular weight of calcium carbonate, V the volume of solution, and $[Ca^{2+}]$ the molar concentration of calcium ion. Assuming rhombohedral morphology for calcite crystals, the value of $f_s/3f_v$ is close to 2. Substituting this value and eq 11 into eq 10, the linear growth rate becomes

$$G = \frac{dL}{dt} = \frac{2MV}{\rho_s A}\left(-\frac{d[Ca^{2+}]}{dt}\right) \quad (12)$$

Equation 12 describes the linear growth rate as a function of calcium ion concentration. Once the concentration profile of calcium ion is available, the linear growth rate can be calculated at any instance of an experiment. Obviously, this simplified method can not be used for thiphasic gas−liquid−solid systems under high gas pressure and temperature. Because the ex situ measurements of calcium ion concentration generally carried out at ambient temperature after filtration, cooling, and degasification are not representative of in situ calcium ion concentration behavior during nucleation/growth of calcite. Moreover, the above cited model considers only rhombohedral morphology for calcite, scalenohedral morphology, axial elongations, and complex agglomeration are then excluded. For these reasons, we propose in the present study a new method to estimate the linear growth initial rate of submicrometric calcite by using Rietveld refinements of X-ray diffraction (XRD) patterns. The calcite crystals were produced in a triphasic gas−liquid−solid system under high gas pressure (55 and 90 bar) and moderate and high temperature (30 and 90 °C). Herein, Rietveld refinements of XRD patterns allowed the calculation of the coherent domain average size r (nm) of calcite precipitates. These experimental−calculated data were then correlated with duration of the reaction t (s) (r vs t). Finally, a kinetic pseudo-second-order model was satisfactory used to fit the data and estimate the linear growth initial rate of submicrometric calcite. For this approach, the concentration profile of calcium ion during calcite growth was not necessary to estimate the linear growth rate, and the crystal morphology was not a limitative condition.

2. Materials and Methods

2.1. Growth of Calcite in a Thiphasic Gas−Liquid−Solid System (Stirred Reactor). One liter of high-purity water with electrical resistivity of 18.2 MΩ·cm and 74.1 g of commercial calcium hydroxide (provided by Sigma-Aldrich) with 96% chemical purity (3% $CaCO_3$ and 1% other impurities) were placed in a titanium reactor (autoclave with internal volume of two liters). The hydroxide particles were immediately dispersed with mechanical agitation (400 rpm). The dispersion was then heated to 90 °C with a heating jacket adapted to the reactor. When the dispersion temperature was reached, 80.18 g of CO_2 with 99.995% chemical purity (provided by Linde Gas S.A.) were injected in the reactor and the total pressure in the system was immediately adjusted to 90 bar by argon injection. Under these pressure−temperature conditions, the vapor phase consists mainly of an $Ar + CO_2$ mixture with the CO_2 in a supercritical state. In order to estimate the linear growth rate of calcite, five different durations of reaction were considered (0.25, 0.5, 4, 15, and 24 h). The experiments were also carried out at 30 °C and 55 bar for reaction durations of 0.25, 4, and 24 h. For this second case, 96.05 g of CO_2 was initially injected in the reactor. At 55 bar and 30 °C, the vapor phase consists mainly of compressed gaseous CO_2. A complete description on the experiments and samples recovery/preservation was reported by Montes-Hernandez et al.[25]

2.2. X-ray Diffraction Analysis of the Solid Phase. X-ray Powder Diffraction (XRD) analyses were performed using a Kristalloflex 810, SIEMENS diffractometer in Bragg−Brentano geometry. The XRD patterns were collected using Co kα_1 ($\lambda_{k\alpha1}$ = 1.7889 Å) and kα_2 ($\lambda_{k\alpha2}$ = 1.7928 Å) radiation in the range $2\theta = 5-80°$ with a step size of 0.02° and a counting time of 8 s per step.

The widths of the diffraction peaks in a diffraction pattern are mainly affected by two contributions: (1) the instrumental resolution and (2) microstructural effects related to the size of the crystallites or to the strains within their crystal structure. Both effects are convoluted in a diffraction pattern but can be separated by the use of convolution or deconvolution methods. A convolution method (Rietveld refinement) has been used in this study to accountz for size and strain effects. For this purpose, an X-ray diffraction pattern of a microstructure-free sample (SiO_2 in our case) has been measured, in order to isolate the instrumental resolution effect. In this way, further Rietveld refinements of the samples using size and strain models account only for microstructural effects.

To get a more detailed knowledge on the texture of the calcite particles, we have performed microstructural analyses within the Rietveld refinement of the X-ray diffraction data. The method is sensitive to the anisotropy of the crystallites, as a refinement of the full X-ray pattern is performed, which includes reflections of different reciprocal space directions. Rietveld refinement of the powder diffraction patterns has been carried out using the FullProf package (Windows version, February 2007).[26] The pseudo-Voigt

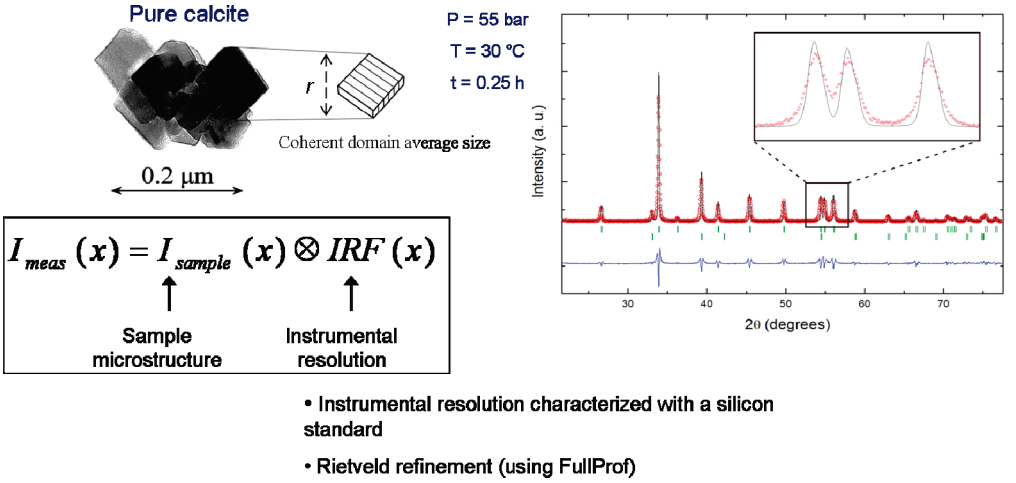

Figure 1. (a) Schematic representation for Rietveld refinement method of each X-ray diffraction pattern, allowing the calculation of coherent domain average size, r (nm).

profile function of Thompson, Cox, and Hastings[27] was used to fit the peak shapes. The parameters constituting the angular-dependent microabsorption correction were refined for each sample. Multiphase analysis was performed introducing a portlandite phase (calcium hydroxide) in the samples when the portlandite to calcite phase transition was not completely accomplished. Structural refinements of calcite were performed considering the $R\bar{3}C$ space group and taking as initial values those obtained in the X-ray powder diffraction study reported by Maslen et al.[28] Scale factor, zero point, cell dimensions, atomic coordinates, and Debye−Waller factors were refined. Background was refined by adjusting a fourth-order polynomial. The instrumental contribution to peak broadening was determined with a SiO_2 sample. [29] The asymmetry parameters of the L. Finger correction S_L and S_D, [30] and the Cagliotti parameters[31] were refined for the standard sample of SiO_2 and kept fixed during the refinements of the calcite patterns. Anisotropic size broadening was modeled in terms of spherical harmonics, and the coherent domain average apparent size along each reciprocal lattice vector was calculated. Coherent domain average size was calculated averaging the resulting size of each of the reciprocal space distances measured. A schematic representation of this refinement method for each X-ray pattern is reported in Figure 1. The Cagliotti parameter U was refined in order to account for some isotropic strain in the Gaussian component of the peak profile. The strain is given in %%: a strain of x %% means a strain ratio of $\varepsilon = (d_i - d_f)/d_i \times 10\,000$, with d_i and d_f being the strain-free crystallite size and the strained crystallite size, respectively. Errors in size and strain have been estimated by performing refinements with different starting points, thus probing the stability of the result. Errors in size and strain are better than 10%.

2.3. Size and Morphology of Calcite Crystals. Isolated fine particles (oriented on carbon Ni grids) of calcite powder were studied using a JEOL 3010 Transmission Electron Microscope (TEM) equipped with an energy-dispersive X-ray analyzer (EDS) to image the morphology and size of calcite crystals.

3. Results and Discussion

3.1. General Comments. In two previous publications by Montes-Hernandez et al.,[25,32] it was demonstrated that the hydrothermal carbonation of calcium hydroxide ($Ca(OH)_2$) at high pressure of CO_2 (initial $P_{CO2} = 55$ bar) and moderate to high temperature (30 and 90 °C) led the formation of submicrometric particles of calcite (< 1 μm). This method allowed a high carbonation efficiency (about 95% of $Ca(OH)_2$-$CaCO_3$ conversion), a significant production rate (48 kg/m^{3}h), and high purity of product (about 96%). It was also demonstrated that the pressure (P), temperature (T), and dissolved amount of CO_2 (x) had significant effects on the average particle size, specific surface area, initial mass growth rate, and the morphology of calcium carbonate crystals. In contrast, these $P-T-x$ conditions used had insignificant effects on the carbonation efficiency of $Ca(OH)_2$. Concerning the calcite-crystal morphology, a preferential precipitation/growth of submicrometric particles of calcite (< 1 μm) with rhombohedral morphology was observed at 90 °C and 90 bar, whereas a preferential precipitation/growth of nanometric particles of calcite (< 0.2 μm) with scalenohedral morphology was observed at 30 °C and 55 bar (see Figure 2). Here, the mass growth rate was globally proportional to amount of dissolved CO_2. This could justify a higher mass growth rate of calcite at lower temperature (see Figure 3). In fact, the mass growth rate of calcite at 30 °C and 55 bar was equal to 15.9 mol/h, whereas the mass growth rate of calcite at 90 °C and 90 bar was equal to 4.3 mol/h. The variation of precipitated calcium carbonate with the reaction time was estimated by a masse balance method. For more details on the data fitting and on the calculation of mass growth rate, see Montes-Hernandez et al. [25]

3.2. Estimation of Linear Growth Initial Rate of Calcite. In a discontinuous reactor, the nucleation rate is related to the particle number concentration while the crystal growth rate is related to the variation of the crystal size with time. During precipitation process, new particles are created by nucleation events. The rate of nucleation can play an important role on the final characteristics of the solid. However, this step remains the most difficult and the lesser studied because the size of particles involved. With new developments in the measurements of sizes of fine particles, some authors attempted to study this process experimentally (e.g., ref 33 and references therein). In the past decade, the simultaneous determination of nucleation and growth rates from batch spontaneous precipitation has been proposed by Aoun et al.[33] Unfortunately, this method is difficultly applied to the triphasic gas−liquid−solid systems because this method was based on the in situ simultaneous measurements of the concentration (by a conductometer) and the crystal size distribution (by a laser diffraction granulometer) during a batch spontaneous precipitation (solution-solution interaction) under atmospheric pressure−temperature conditions. For our

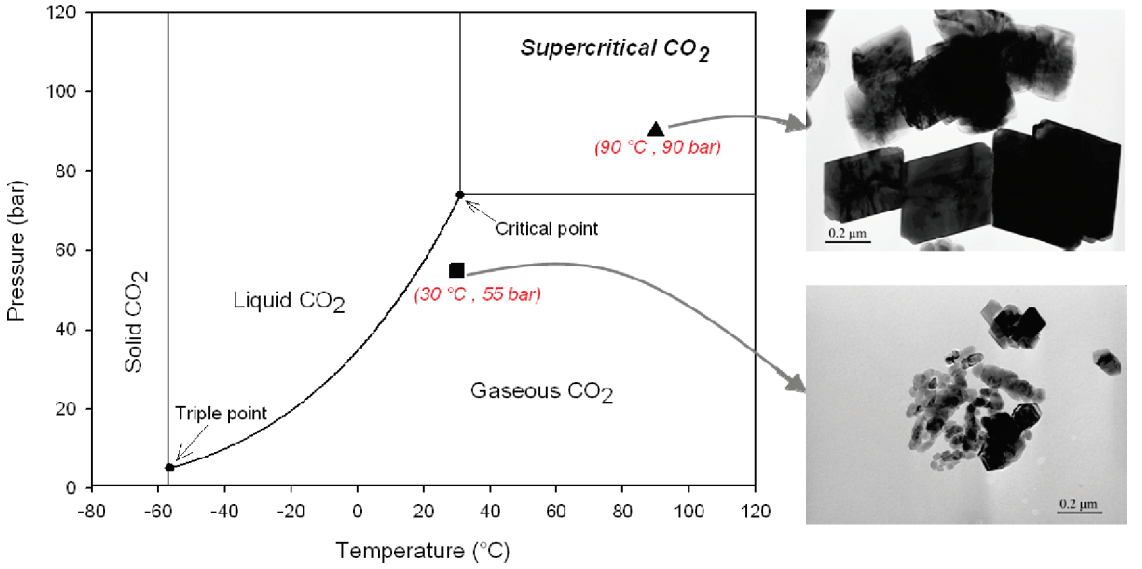

Figure 2. Experimental conditions represented on a pressure−temperature phase diagram for carbon dioxide. Submicrometric particles of calcite (< 1 μm) with rhombohedral morphology were grown at 90 °C and 90 bar, whereas nanometric particles of calcite (< 0.2 μm) with scalenohedral morphology were grown at 30 °C and 55 bar.

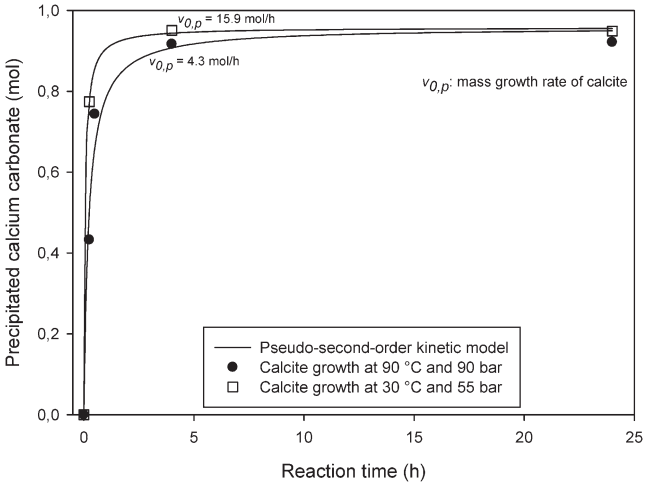

Figure 3. Kinetic behavior of calcite growth in a triphasic gas−liquid−solid system under high gas pressure (55 and 90 bar) and moderate to high temperature (30 and 90 °C). Here, the precipitated calcium carbonate was estimated by a masse balance method. For more details on the data fitting and on the calculation of mass growth rate, see Montes-Hernandez et al.[25]

Table 1. Coherent Domain Average Size (r) estimated by Using Rietveld Refinement of X-ray Diffraction Patterns (powder diffraction data); Error for All Values Is Better than 10%

P (bar)	T (°C)	reaction time, t (s)	r (nm)[a]
55	30	900	42
		14400	59
		86400	64
90	90	900	112
		1800	99
		14400	157
		54000	157
		86400	185

[a] r = Coherent domain average size.

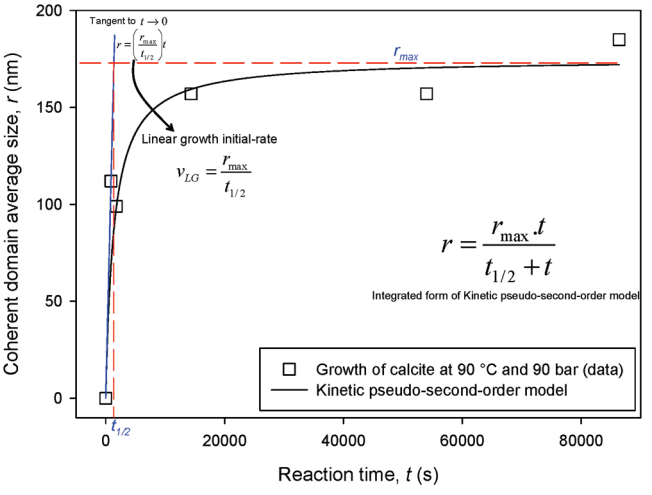

Figure 4. Graphical representation of linear growth initial rate of submicrometric calcite produced in a triphasic gas−liquid−solid system.

experiments, the nucleation step was not isolated from the growth process; in fact, the ex situ measurements on the variation of the crystal size with reaction time were performed by using the Rietveld refinement of each X-ray pattern. This refinement method allowed such the estimation of coherent domain average size as a function of reaction time ($r = f(t)$) (see Table 1 and subsection 2.2). Here, a kinetic pseudosecond-order model was satisfactory used to describe the growth process of calcite in a triphasic gas−liquid−solid system. Finally, the fitting parameters allowed the calculation of linear growth initial rate of calcite. Note that a kinetic pseudo-second-order model predicts a fast mass transfer followed by a slow equilibration of mass transfer in closed systems. The differential form for this kinetic model can be written as follows

$$\frac{dr}{dt} = k_G(r_{max} - r)^2 \qquad (13)$$

where k_G is the rate constant of calcite-crystal growth [1/nm s], r_{max} is the maximum of coherent domain average size

at equilibrium [nm], and r is the coherent domain average size at any time, t [nm].

The integrated form of eq 13 for the boundary conditions $t = 0$ to $t = t$ and $r = 0$ to $r = r$ is represented by a hyperbolic relationship

$$r = \frac{r_{max} t}{\left(\frac{1}{k_G r_{max}}\right) + t} \quad (14)$$

Note that the rate constant k_G (1/nm s) has no physical interpretation. For this reason, a new parameter can be defined, $1/(k_G r_{max}) = t_{1/2}$, which represents the duration after which half of the maximum of coherent domain average size was obtained. In the current study, $t_{1/2}$ is called "half-growth time" and can be used to calculate the linear growth initial rate of calcite, v_{LG} [nm/s] by using the following expression

$$v_{LG} = \frac{r_{max}}{t_{1/2}} = k_G (r_{max})^2 \quad (15)$$

Graphically, the linear growth initial-rate v_{LG} is defined as the slope of the tangent line when the time t tends toward zero on the r vs t curve (see Figure 4).

The fitting of kinetic data (r vs t) by using eq 14 allows the estimation of $t_{1/2}$ and r_{max} parameters. Here, a nonlinear regression by the least-squares method was performed. In the Figure 5, the experimental−calculated data and fitting curves are reported. Moreover, the fitting parameters ($t_{1/2}$ and r_{max}), the linear growth rate of calcite (v_{LG}) (calculated by eq 15), and the correlation factor values are summarized in Table 2. These results revealed that the values of linear growth rate of calcite were equivalents for both systems, 0.14 nm/s at 30 °C and 55 bar and 0.12 nm/s at 90 °C and 90 bar. However, the average size of calcite crystals, here expressed as a maximum of coherent domain average size, was clearly higher at 90 °C and 90 bar (174 nm) than at 30 °C and 55 bar (63 nm). This particular characteristic on the crystal size is in agreement with TEM (transmission electron microscope) observations (see Figure 2). Note that the variation on the average size of calcite crystals with reaction time could also provide relevant information on the

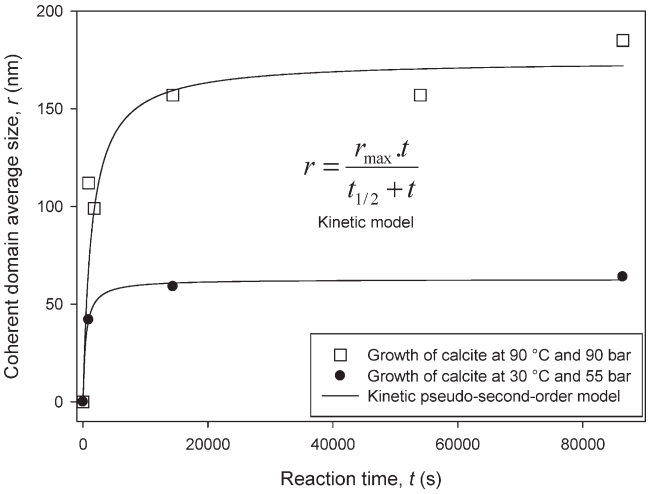

Figure 5. Kinetic behavior of calcite growth in a triphasic gas−liquid−solid system under high gas pressure (55 and 90 bar) and moderate to high temperature (30 and 90 °C). Note that the domain coherent average size was estimated by using Rietveld refinements of X-ray diffraction patterns. The fitting parameters and the linear growth rate of calcite are reported in Table 2.

Table 2. Fitting Parameters Estimated by Eq 14, Linear Growth Initial Rate of Calcite Calculated by Eq 15 and Correlation Factor[a]

$T-P$ system (°C−bar)	r_{max} (nm)	$t_{1/2}$ (s)	v_{LG} (nm/s)	R
30−55	63 ± 2	450 ± 65	0.14000	0.99
90−90	174 ± 10	1394 ± 480	0.12482	0.99

[a] T = temperature, P = pressure, r_{max} = maximum of coherent domain average size, $t_{1/2}$ = half-growth time, v_{LG} = linear growth initial rate of calcite, R = correlation factor.

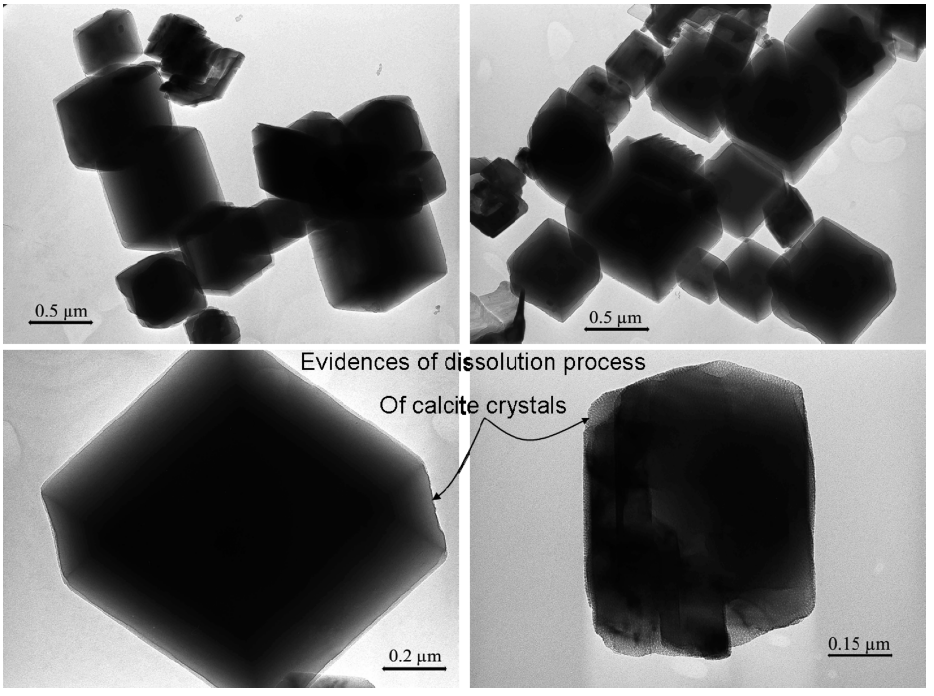

Figure 6. Evidence of a secondary dissolution process of rhombohedral crystals during calcite growth at 90 °C and 90 bar in a triphasic gas−liquid−solid closed system. TEM micrographs.

Table 3. Summary of Growth Rate Values, Produced Calcium Carbonate Weight, and Specific Surface Area of Calcite Growth at High Gas Pressure (55 and 90 bar) and Moderate to High Temperature (30 and 90°C)[a]

$T-P$ system (°C−bar)	$v_{0,p}$ (mol/h)	$S_{BET\ product}$ (m^2/g)	m_{CaCO3} (g)	$v_{0,p\rightarrow LG}$ (nm/s)	v_{LG} (nm/s)
30−55	15.9	9.72	94.9	0.17684	0.14000
90−90	4.3	5.95	92.2	0.08042	0.12482

[a] $v_{0,p}$ = Mass growth rate (see Figure 3 in this study); $S_{BET\ product}$ = specific surface area of product at equilibrium state (see ref 32); m_{CaCO3} = produced calcium carbonate weight (see ref 25); $v_{0,p\rightarrow LG}$ = linear growth rate of calcite deduced from mass growth rate (see eq 16 in this study); v_{LG} = linear growth rate deduced from Rietveld refinement of XRD patterns (see section 3.2 in this study).

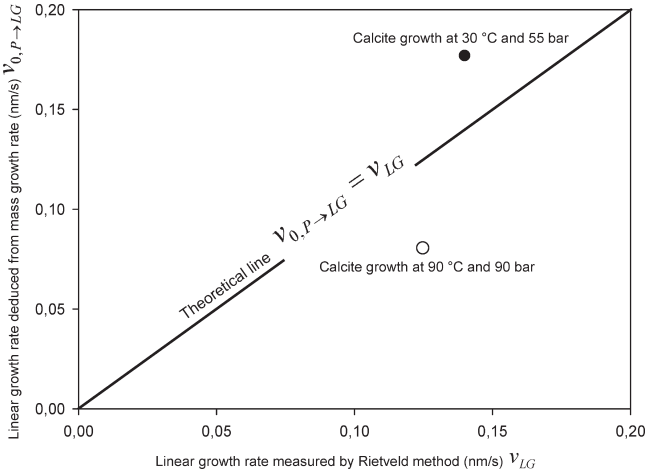

Figure 7. Comparison of linear growth rate values deduced from mass growth rate with linear growth rate values deduced by the average variation of crystal size (i.e., variation in coherent domain average size) as a function of reaction time. Coherent domain average size was determined by Rietveld refinement of X-ray diffraction patterns.

secondary physicochemical processes. For example, the coherent domain average size as detected by X-ray diffraction is accompanied by a dissolution process of the crystallites in their very early stage of nucleation (first 0.5 h). This fact can be clearly observed following the kinetic experimental−estimated data of growing of the crystallites from the XRD coherent domain average size shown in Table 1 and/or Figure 4: they reflect a continuous growing of the average size of the coherent domains at 30 °C and 55 bar (only three points), whereas the average size decreases from 112 to 99 nm when passing from 900 to 1800 s of reaction at 90 °C and 90 bar. This behavior is suspected later in the reaction. This decrease can be interpreted in terms of a dissolution process of calcite crystals, given that there is a molar excess of carbon dioxide with respect to calcium hydroxide in the reactor (CO_2/$Ca(OH)_2$ molar ratio = 1.82) leading to an acidic condition which would explain this behavior. The microscopic observations (by TEM) provide the evidence of a secondary dissolution process of crystals during calcite formation at 90 °C 90 bar in this closed system (Figure 6).

3.3. Masse growth Rate vs Linear Growth Rate. The masse growth rate can be defined as the global mass flux incorporated and/or nucleated at solid−fluid interfaces during crystal growth processes. This mass flux can be related to the particle size in order to deduce the linear growth rate.[24,33,34] This concept was adapted to our measurements reported in Figure 3. For this case, the linear growth rate of calcite from mass growth rate can be deduced as follows

$$v_{0,\mathrm{P}\rightarrow \mathrm{LG}} = \frac{M_{CaCO3}}{\rho_{CaCO3} S_{BETproduct} m_{CaCO3}} v_{0,\mathrm{P}} \qquad (16)$$

where M_{CaCO3}, ρ_{CaCO3}, and m_{CaCO3} are the molecular weight, the density, and the produced weight of calcium carbonate, respectively. The $S_{BET\ product}$ is the specific surface area of product and it is equivalent to specific surface area of calcium carbonate in our experiments (measurements reported in 32), assuming a complete transformation of calcium hydroxide ($Ca(OH)_2$) to calcium carbonate ($CaCO_3$).[25] Note that eq 16 represents only an "a posteriori" calculation, knowing the specific surface area of solid product and the produced calcium carbonate weight at the equilibrium. Obviously, this global calculation not takes into account the temporal variation of the specific surface area of solid during calcite-crystal growth. But, in our experiments was demonstrated that this calculation can be a well approximation to deduce the linear growth rate (see Table 3 and Figure 7). Figure 7 shows the discrepancy of linear growth rate values with respect to theoretical line (with slope = 1). Table 3 summarizes the growth rates values, the produced calcium carbonate weight, and the specific surface areas of calcite growth at high gas pressure (55 and 90 bar) and moderate to high temperature (30 and 90 °C).

4. Conclusion

The main goal for this study was to propose a novel method allowing the estimation of the linear growth rate of calcite in a triphasic gas−liquid−solid system under high gas pressure (55 and 90 bar) and moderate to high temperature (30 and 90 °C). This was successfully reached by using Rietveld refinement of X-ray diffraction patterns. Herein, an average variation of particle size (coherent domain average size) was determined as a function of reaction time. Then, a kinetic pseudo-second-order model was satisfactory used to deduce the linear growth initial rate. The results showed that the values of linear growth rate of calcite were equivalents for both systems, in other words, 0.14 nm/s at 30 °C and 55 bar and 0.12 nm/s at 90 °C and 90 bar. However, the average size of calcite crystals, here expressed as a maximum of coherent domain average size, was clearly higher at 90 °C and 90 bar (174 nm) than at 30 °C and 55 bar (63 nm).

The main advantage for this method is the possibility to estimate the linear growth rate of crystalline fine particles (> 40 nm) growing in triphasic gas−liquid−solid systems. Here, we consider that depressurization of cell reaction has lesser physicochemical effect on the solid precipitates than on the interacting solutions.

Acknowledgment. The authors are grateful to the National Research Agency, ANR (GeoCarbone-CARBONATATION project) and the National Research Council (CNRS), France, for providing financial support for this work. This paper is dedicated by the first author to the memory of his father (Prospero Montes Flores), who died on November 17, 2008, in Amaxac de Guerrero, Tlaxcala, Mexico.

References

(1) Seifritz, W. *Nature* **1990**, *345*, 486.
(2) Lackner, K. S.; Wendt, C. H.; Butt, D. P.; Sharp, D. H.; Joyce, E. L. *Energy* **1995**, *20*, 1153.
(3) Gerdemann, S. J.; O'Connor, W. K.; Dahlin, D.; Penner, L. R.; Rush, H. *Environ. Sci. Technol.* **2007**, *41*, 2587.

(4) Teir, S.; Elovena, S.; Zevenhoven, R. *Energy Convers. Manage.* **2005**, *46*, 2954.
(5) Costa, G.; Baciocchi, R.; Polettini, A.; Pomi, R.; Hills, C. D.; Carey, P. J. *Environ. Monit. Assess.* **2007**, *135*, 55.
(6) Perez-Lopez, R.; Montes-Hernandez, G.; Nieto, J.-M.; Renard, F.; Charlet, L. *Appl. Geochem.* **2008**, *23*, 2292.
(7) Montes-Hernandez, G.; Perez-Lopez, R.; Renard, F.; Nieto, J.-M.; Charlet, L. *J. Hazard. Mater.* **2009**, *161*, 1347.
(8) Montes-Hernandez, G.; Concha-Lozano, N.; Renard, F.; Quirico, E. *J. Hazard. Mater.* **2009**, *166*, 788.
(9) Fujita, Y.; Redden, G. D.; Ingram, J.; Cortez, M. M.; Ferris, G.; Smith, R. W. *Geochim. Cosmochim. Acta* **2004**, *68*, 3261.
(10) Freij, S. J.; Godelitsas, A.; Putnis, A. *J. Cryst. Growth* **2005**, *273*, 535.
(11) Gower, L. A.; Tirrell, D. A. *J. Cryst. Growth* **1998**, *191*, 153.
(12) Jonasson, R. G.; Rispler, K.; Wiwchar, B.; Gunter, W. D. *Chem. Geol.* **1996**, *132*, 215.
(13) Chrissanthopoulos, A.; Tzanetos, N. P.; Andreopoulou, A. K.; Kallitsis, J.; Dalas, E. *J. Cryst. Growth* **2005**, *280*, 594.
(14) Menadakis, M.; Maroulis, G.; Koutsoukos, P. G. *Comput. Mater. Sci.* **2007**, *38*, 522.
(15) Dousi, E.; Kallitsis, J.; Chrisssanthopoulos, A.; Mangood, A. H.; Dalas, E. *J. Cryst. Growth* **2003**, *253*, 496.
(16) Pastero, L.; Costa, E.; Alessandria, B.; Rubbo, M.; Aquilano, D. *J. Cryst. Growth* **2003**, *247*, 472.
(17) Lee, Y. J.; Reeder, R. *Geochim. Cosmochim. Acta* **2006**, *70*, 2253.
(18) Temmam, M.; Paquette, J.; Vali, H. *Geochim. Cosmochim. Acta* **2000**, *64*, 2417.
(19) Dalas, E.; Chalias, A.; Gatos, D.; Barlos, K. *J. Colloids Interface Sci.* **2006**, *300*, 536.
(20) Teng, H. H.; Dove, P. M.; Orme, C. A.; De Yoreo, Y. J. *Science* **1998**, *282*, 724.
(21) Paquette, J.; Reeder, R. J. *Geochim. Cosmochim. Acta* **1995**, *59*, 735.
(22) Deleuze, M.; BrantleyS, L. *Geochim. Cosmochim. Acta* **1997**, *61*, 1475.
(23) Nehrke, G.; Reichard, G. J.; Van Cappellen, P.; Meile, C.; Bijima, J. *Geochim. Cosmochim. Acta* **2007**, *71*, 2240.
(24) Chen, P.-C.; Tai, C. Y.; Lee, K. C. *Chem. Eng. Sci.* **1997**, *52*, 4171.
(25) Montes-Hernandez, G.; Renard, F.; Geffroy, N.; Charlet, L.; Pironon, J. *J. Cryst. Growth* **2007**, *308*, 228.
(26) Rodriguez-Carvajal, J. *Collected Abstracts of Powder Diffraction Meeting*; Toulouse, France, July 1990 ; Galy, J. , Ed.; International Union of Crystallography: Chester, U.K., 1990.
(27) Thompson, P.; Cox, D. E.; Hastings, J. B. *J. Appl. Crystallogr.* **1987**, *20*, 79.
(28) Maslen, E. N.; Streltsov, V. A.; Streltsova, N. R. *Acta Crystallogr., Sect. B* **1993**, *49*, 636.
(29) Reference no. 00−046−1045 from JCPDS, International Centre for Diffraction Data.
(30) Finger, L. W.; Cox, D. E.; Jephcoat, A. P. *J. Appl. Crystallogr.* **1994**, *27*, 892.
(31) Cagliotti, G.; Paoletti, A.; Ricci, F. P. *Nucl. Instrum. Methods Phys. Res.* **1958**, *3*, 223.
(32) Montes-Hernandez, G.; Fernandez-Martinez, A.; Charlet, L.; Tisserand, D.; Renard, F. *J. Cryst. Growth* **2008**, *310*, 2946.
(33) Aoun, M.; Plasari, E.; David, R.; Villermaux, J. *Chem. Eng. Sci.* **1999**, *54*, 1161.
(34) Nielsen, A. E. *Acta Chem. Scand.* **1958**, *12*, 951.